Plasma Sources Sci. Technol. **5** (1996) 499–509. Printed in the UK

# Spatial distributions of power and ion densities in RF excited remote plasma reactors

**Irène Pérès† and Mark J Kushner‡**

University of Illinois, Department of Electrical and Computer Engineering, 1406 W Green Street, Urbana, IL 61801, USA

Received 7 February 1995, in final form 24 December 1995

**Abstract.** Remote plasma systems operating at moderate pressures (tens to hundreds of milli-Torr) are being developed for use in deposition and etching of microelectronics materials. In particular, remote plasma-enhanced chemical vapour deposition (RPECVD) has been investigated for fabrication of $\mu$c-Si, $Si_3N_4$ and $SiO_2$ films, as well as for plasma cleaning and passivation. RPECVD reactors typically consist of a narrow upstream plasma zone and a wide downstream deposition chamber. A sub-set of the reactants is made to flow through the upstream plasma zone, creating excited states which are mixed with additional reactants injected into the downstream deposition chamber. RPECVD systems are typically excited by a radio frequency electric field produced by a coil surrounding the upstream plasma zone with the intent of generating a plasma that is well confined to the upstream zone. It is common, however, for the plasma to extend downstream towards the substrate due to stray inductive fields and capacitive coupling. In this paper, a computer model for remote plasma reactors is described, with which the spatial distributions of power deposition and ion densities are investigated. The characteristics of remote plasma reactors are presented and the influences of the operating conditions (geometry, gas pressure and RF frequency) on plasma confinement are investigated for He, $O_2$ and He–$SiH_4$ mixtures.

## 1. Introduction

Traditional plasma processing reactors for deposition of microelectronics materials have the substrate located either in, or in close proximity to, the plasma [1]. Although this arrangement produces high deposition rates, the pre-mixed feedstock gases are uncontrollably dissociated in the plasma zone and therefore little control of precursor fluxes to the substrates is afforded. In addition, energetic particles (ultraviolet photons, ions or hot atoms) can impact upon the substrate, leading to damage of the growing film. To address these conditions, remote plasma-enhanced chemical vapour deposition (RPECVD) has been developed [1–3].

RPECVD reactors consist of a narrow upstream plasma tube and a wider downstream deposition chamber (see figure 1). The plasma is generated by a coil wrapped around the upstream tube. Non-deposition gases (or a sub-set of the deposition gases) are made to flow through the plasma zone. Radicals and excited states produced in the plasma zone advect or diffuse downstream, where (additional) deposition gases are injected. Reactions between the plasma-generated radicals and excited states and the injected gases produce the deposition precursor species, which then flow to the substrate. By careful selection of the position of the injection nozzles, flow rates and location of the substrate, the injected deposition gases can be isolated from the plasma zone. In doing so, deposition precursors are produced predominantly by chemical reactions between the activated and injected gases. This affords a more selective production of precursors than one obtains by direct electron impact dissociation of the deposition gases. For example, RPECVD of $SiO_2$ is performed by passing a He–$O_2$ or He–$N_2O$ mixture through the plasma zone and injecting $SiH_4$ downstream. Typical conditions are gas pressures of tens to hundreds of milli-Torr, flow rates of tens to hundreds of sccm (residence times of tens to a hundred milliseconds) and power deposition of tens of watts.

In practice, confinement of the plasma to the upstream zone resulting in true isolation of the injected gases from the plasma is difficult to achieve. With high power deposition, the inductively coupled electric field may be strong enough to allow the plasma to sustain itself beyond the limits of the coil. The inductive voltage drop across the coil can also capacitively couple to earth planes in the deposition chamber (such as the injection nozzle or substrate). These capacitively coupled fields can be large enough to sustain

† Present address: Département de Physique, Université de Montréal, CP 6128, Succursale A, Montréal, Québec, Canada H3C 3J7.
‡ Author to whom correspondence should be addressed. E-mail: mjk@uluc.edu

0963-0252/96/030499+11$19.50  

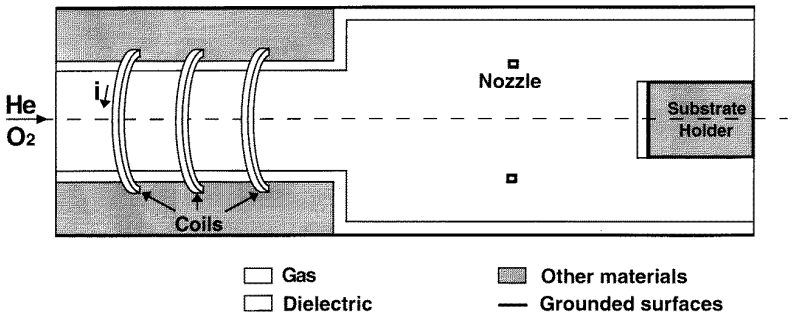


**Figure 1.** A schematic diagram of the remote plasma reactor (RPR) used in this study. The plasma is sustained by a coil powered at radio frequencies, wrapped around the upstream chamber. The gas is typically made to flow through the plasma zone and exhausted by the substrate holder. Earthed gas injection nozzles are located in the downstream chamber.

a plasma in the downstream chamber or affect plasma transport.

In this paper, we describe a computer model of remote plasma reactors (RPRs) to investigate the spatial distributions of power deposition and ion densities resulting from various coil positions and operating conditions. The study focuses on the generation and transport of the plasma and does not discuss the details of the deposition chemistry. Results from the model will be used to identify operating regimes in which the plasma largely remains confined to the upstream plasma zone and regimes in which significant penetration of the plasma occurs downstream. The model is described in section 2, followed by a discussion of results for operating RPRs using He, $O_2$ and He–$SiH_4$ chemistries in section 3. Our concluding remarks are in section 4.

## 2. A description of the model

Our model geometry is patterned after the RPECVD reactor described by Lucovsky *et al* [2]. The RPR consists of an upstream plasma tube 15 cm long and 4 cm in diameter feeding into a 20 cm long, 12 cm diameter deposition chamber. The walls of the plasma tube and deposition chamber are quartz. A cylindrical earthed substrate holder is located at the base of the deposition chamber and, when used, an earthed gas injection ring is located approximately 5 cm from the throat of the plasma zone. A helical coil powered at RF frequency (5–100 MHz) is wrapped around the plasma tube.

The model is a two-dimensional cylindrically symmetrical hybrid simulation of the electromagnetic and electrostatic fields in the reactor and of plasma and neutral species kinetics in a RPR. The model consists of two modules, the electromagnetics module (EM) and the fluid-chemistry module (FCM). These modules are iterated until a quasi-steady state solution has been obtained. There are three timescales of interest; the RF period (74 ns), the time required for ions and excited states to equilibrate in the plasma zone (tens of microseconds) and the time required for neutral radicals produced in the plasma zone to diffuse downstream (tens of milliseconds). These disparate timescales have been addressed by using two levels of acceleration or 'predictor–corrector' techniques. The flow of the model will be briefly discussed.

Prior to beginning execution of the model, excitation rate coefficients are computed for the gas mixture of interest by solving Boltzmann's equation for the electron energy distribution (EED) using a two-term spherical harmonic expansion. EEDs were computed over a wide range of $E/N$ (electric field/number density), and the resulting transport and rate coefficients were entered into a 'look-up' table for use during execution of the model. The model then begins by specifying a plasma conductivity as a function of position and a total power deposition by the inductive electric field. The inductively coupled electric fields produced by the helical coil are then obtained throughout the volume of the RPR using the EM. Due to the symmetry of the RPR and coils, the inductively coupled electric field has only an azimuthal component $E_\theta$ which is a function of position $(r, z)$. These fields are transferred to the FCM. In the fluid-chemistry module, continuity equations for all charged and neutral species and Poisson's equation are solved as functions of $(r, z)$ and time. Electron transport coefficients and electron impact rate coefficients are obtained from the previously prepared 'look-up' table using a modified local field approximation. After a specified time of integration, the plasma conductivity as a function of $(r, z)$ is transferred back to the EM. The procedure is repeated, iterating between the EM and FCM, until the species densities converge to the quasi-steady state.

### 2.1. The electromagnetics module

The EM is essentially the same as used in the model discussed in [5] and so will be only briefly described here. Due to the symmetry of the coil surrounding the plasma tube, the inductively coupled electric field has only an azimuthal component. We assume that the electric field is purely sinusoidal at frequency $\omega$ and given by

$$E_\theta(\boldsymbol{r}, t) = E_\theta(\boldsymbol{r})\, \mathrm{e}^{\mathrm{i}\omega t} \tag{1}$$

where $E_\theta(\boldsymbol{r})$ is the complex amplitude of the azimuthal electric field. This amplitude is obtained by solving the complex wave equation in the body of the plasma,

$$\nabla^2 E_\theta(\boldsymbol{r}) = \mathrm{i}\omega\sigma(\boldsymbol{r}) E_\theta(\boldsymbol{r}) \tag{2}$$

where $\sigma$ is the plasma conductivity. The method of solution is patterned after Yu and Girshik [6] and is explained in [5].

We specify the total power deposition in the plasma by the inductive field and adjust the coil current to obtain this value.

The boundary conditions for the electric field used in the EM are that $E_\theta$ is zero on earthed metallic surfaces and zero on the axis due to symmetry. At the inlet and outlet of the RPR, we assume continuity of the field by specifying that $\partial^2 E_\theta/\partial z^2 = 0$.

### 2.2. The fluid-chemistry module

In the FCM, the continuity equations for all charged and neutral species are integrated and Poisson's equation is solved for the electrostatic electric field. The equation that we solve for species $i$ is

$$\frac{\partial N_i}{\partial t} = -\nabla(q_i \mu_i \boldsymbol{E}_s - D\nabla N_i) + S_i \tag{3}$$

where $N_i$ is the density of species $i$, $q_i$ is the charge, $\mu_i$ is the mobility, $D_i$ is the diffusion coefficient and $S_i$ is the local source function of species $i$. $\boldsymbol{E}_s$ is the electrostatic field. All quantities are functions of $(r, z)$. The source function represents the change in density due to collisional processes, including electron impact ionization, excitation, recombination and heavy-particle reactions. The electric field is obtained from solution of Poisson's equation in the manner described below.

The electron transport coefficients and impact rate coefficients in equation (3) are obtained by calculating an effective local electric field/number density, $(E/N)'$, which is then used to extract the necessary coefficients from the previously constructed 'look-up' table. $(E/N)'$ accounts for excitation both from the inductive azimuthal and from the $(r, z)$ electrostatic field and is defined by

$$P(\boldsymbol{r}) = \sigma(\boldsymbol{r})[(E/N)']^2 N^2 \tag{4}$$

where $P$ is the total power deposition and $\sigma$ is the plasma conductivity. The plasma conductivity is

$$\sigma = \frac{\sigma_0}{1 + (\omega/\nu_m)^2} \tag{5}$$

where $\sigma_0$ is the dc conductivity and $\nu_m$ is the electron momentum transfer collision frequency. The power deposition is obtained from

$$P(\boldsymbol{r}, t) = \sigma[E_\theta(\boldsymbol{r})\sin(\omega t)]^2 + \sum_i \frac{q_i}{e}(\mu_i N_i \boldsymbol{E}_s - D_i \nabla N_i)\cdot \boldsymbol{E}_s. \tag{6}$$

The first term in equation (6) accounts for power deposition from the azimuthal electric field $E_\theta$. The second term in equation (6) accounts for net power deposition from the electrostatic field $\boldsymbol{E}_s$. In the steady state, in the absence of capacitive coupling, there will be no power deposition by the electrostatic field ($(r, z)$ in this case) if that field results totally from ambipolar transport since the net current is by definition zero. The analogue to this situation is a cylindrical positive column discharge in which the power is deposited by the axial electric field but there is no net power coming from the large radial ambipolar field. When capacitive coupling is added, then there can be net power deposition by the $(r, z)$ electrostatic fields.

The use of the local field approximation (LFA) in generating rate and transport coefficients was chosen due to the long time scales required for the solution to converge and the increased computation cost of a kinetics scheme. The LFA is a reasonable approximation for predominantly inductively coupled plasmas in which the net electric fields do not exceed a few V cm$^{-1}$. These conditions are generally satisfied in our study (tens to hundreds of milli-Torr, 13.56 MHz). In purely inductively coupled cylindrical systems, however, the electric field on the axis is zero due to symmetry. Therefore using the LFA causes an unrealistically large gradient in transport coefficients near the axis. This gradient would not otherwise exist had, for example, energy transport been included. The modulation of transport coefficients during the RF cycle is also of concern. It has been shown by others [7] that, for the pressures of interest, the tail of the EED oscillates during the RF cycle, causing modulation of inelastic electron impact rate coefficients. The lower energy bulk portion of the EED and hence the electron temperature does not appreciably oscillate during the RF cycle. To account for these effects, the $E/N$ that we used to obtain our transport coefficients is defined by

$$\left(\frac{E(\boldsymbol{r}, t)}{N}\right)_e = \int\int \left(\frac{E}{N}\right)'(\boldsymbol{r}, t) g(\boldsymbol{r}, \boldsymbol{r}') h(t, t')\, \mathrm{d}\boldsymbol{r}'\, \mathrm{d}t'. \tag{7}$$

In equation (7), $g(\boldsymbol{r}, \boldsymbol{r}')$ is a spatial averaging function whose extent is defined by the electron momentum equilibration distance, typically only one numerical cell, employed to remove the unphysical gradients in transport coefficients predicted by the LFA. The function $h(t, t')$ is a time average over the immediately preceding RF cycle, and $(E/N)'$ is defined by equation (4). In doing so, the bulk electron temperature and mobility are essentially constant in time at a given $(r, z)$. Rate coefficients for high-threshold inelastic processes are obtained using the real-time $E/N$ in order to represent the variation of rates of inelastic processes through the RF cycle more accurately.

Poisson's equation is solved throughout the volume of the RPR. In specifying the geometry, we also specify material properties as being either conductors or dielectrics with locally dependent permittivities. Potential boundary conditions are specified on all metal surfaces. The form of Poisson's equation that we solve is

$$\nabla \cdot \varepsilon \nabla \Phi = \rho \tag{8}$$

where $\Phi$ is the electric potential, $\varepsilon$ is the permittivity and $\rho$ is the volumetric charge density. The boundary conditions along the dielectric walls are included, either for radially or for axially oriented surfaces, by applying Gauss's law

$$(\varepsilon \boldsymbol{E}\cdot\hat{n})_1 - (\varepsilon \boldsymbol{E}\cdot\hat{\boldsymbol{n}})_2 = \sigma_s \tag{9}$$

where $\boldsymbol{E}\cdot\hat{\boldsymbol{n}}$ is the component of the electric field normal to the surface separating media 1 and 2 which have permittivities $\varepsilon_1$ and $\varepsilon_2$, respectively. The surface charge density, $\sigma_s$, is obtained by integrating the charged particle

fluxes to surfaces in contact with the plasma with respect to time:

$$\sigma(t) = \sum_i \int_0^t q_i(\boldsymbol{f}_i(t') \cdot \hat{\boldsymbol{n}})\,\mathrm{d}t'. \tag{10}$$

In equation (10), the sum is over charged species $i$ having flux $\boldsymbol{f}_i$ to the surface with normal $\hat{\boldsymbol{n}}$. The electric potential on the corners of the dielectric walls is obtained by applying Gauss's law to both surface elements adjacent to the corner.

The substrate and the outer wall are earthed and define the zero potential. One end of the coil is typically earthed and the opposite end is driven at the specified RF frequency. Unless otherwise noted, the inductive voltage drop across the coil is linearly distributed along its length. The amplitude of the RF voltage is determined by the applied current and the inductance of the coil. The inductance of the coil is obtained using the method of Grover [8].

Poisson's equations and the boundary equations defined by equation (9) are simultaneously solved using a semi-implicit form of the method of successive over-relaxation (SOR). In this technique, we include a prediction of the volume and surface charge densities at the time at which the electric potential will be used:

$$\rho(t + \Delta t) = \rho(t) + \Delta t \frac{\partial \rho}{\partial t} \tag{11a}$$

$$\sigma_s(t + \Delta t) = \sigma_s(t) + \Delta t \frac{\partial \sigma_s}{\partial t}. \tag{11b}$$

The time rate of change of the charge density, $\partial\rho/\partial t$ can be expressed as a function of the potential and the densities of charged species as

$$\rho(t + \Delta t) = \rho(t) + \Delta t \sum_i [-q_i \nabla \cdot (-q_i \mu_i \nabla \Phi - D_i \nabla N_i)]. \tag{12}$$

The expression for surface charge density that we use is

$$\sigma_s(t + \Delta t) = \sigma_s(t) + \Delta t \sum_i [-q_i(-q_i \mu_i \nabla \Phi - D_i \nabla N_i)]. \tag{13}$$

The mathematical details of solving Poisson's equation using these charge densities are discussed in [5].

### 2.3. The acceleration methodology

The continuity equations and Poisson's equation are discretized over a uniform mesh using conservative donor cell finite differences. The mesh typically consisted of 31 radial and 71 axial points for the standard reactor. The semi-implicit scheme previously described allowed us to integrate the continuity equations over time steps larger than the dielectric relaxation time step. However, time steps are typically limited to between 0.02 and 0.001 times the RF cycle to resolve the oscillations of the capacitive fields. Given this restriction in time step, a prohibitively large amount of computer time would be required to achieve quasi-steady state conditions for all species. To obtain the quasi-steady state, two acceleration techniques were employed.

The first acceleration technique addresses the time required for the plasma in the upstream tube to achieve a quasi-steady state, which is typically tens of microseconds. The continuity and Poisson equations are directly integrated in time for a few RF cycles. The cycle-averaged time rates of change of numbers of charged and neutral species are computed and the solution is 'projected' to future times by performing a single first-order update using a large $\Delta t$. Algorithms are employed which limit the fractional increases or decreases in densities. After the acceleration step, there is no guarantee that charge neutrality has been maintained. The charge densities are therefore re-normalized (using the sum of the positive ion densities as a reference) to be charge neutral at all locations and the surface charge is removed from the dielectric surfaces. The integration is then re-started with these new values of densities and surface charges. Using this technique, the calculation essentially begins anew. Since the ambipolar fields re-establish themselves in a fraction of the RF cycle, there is little time lost in that regard. The integration in the FCM is typically performed for 20 RF cycles, which represents up to some hundreds of microseconds of 'real time'. The plasma conductivity is then fed back into the EM to update the azimuthal electric field. The integration of the FCM is then re-started. This iterative procedure is repeated until quasi-steady state conditions are obtained, which is achieved, typically, in 35–40 $\mu$s of integration time and many milliseconds of 'real time'.

The convective time scale for neutral species to move from the plasma zone to the substrate is tens of milliseconds, a time which is difficult to span while integrating the plasma transport and Poisson's equation. To reach quasi-steady state conditions for neutral species as well, we use a second stage of acceleration. After the plasma species have reached a quasi-steady state using the method described above, the source functions for the neutral species are averaged over an RF cycle. The continuity equations for neutral species only are then integrated using these cycle-averaged source functions. This acceleration step takes typically 0.1–0.2 s. After this neutral species acceleration, the full plasma transport equation and Poisson's equation are integrated during a few iterations of 20 RF cycles between the FCM and the EM. This procedure is necessary to recover consistency between the neutral and charged particle densities. This last step is necessary only if there is some coupling between the production and losses of neutral and charged species.

## 3. Plasma properties and radical densities in remote plasma reactors

In this section results obtained from this model will be discussed for plasmas sustained in He, $O_2$ and He–$SiH_4$. The species and reactions included in the model are listed in [9, 10]. We will first describe plasma characteristics obtained while varying the geometry of the reactor and coils and suppressing capacitive coupling. We will then discuss the possible influence of charge building up on the walls of the reactor on plasma transport. Finally, we discuss the dependence of the development and expansion of the plasma on power deposition, RF frequency and capacitive coupling.

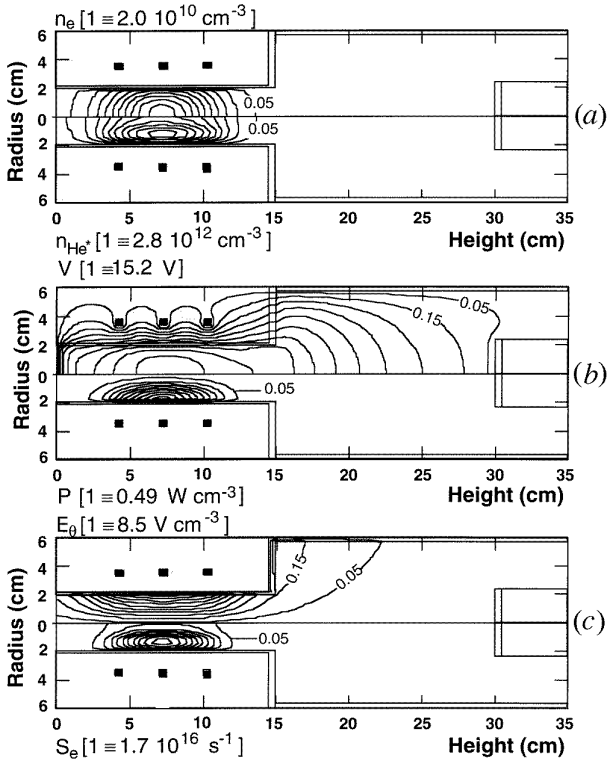


**Figure 2.** Characteristics of a quasi-steady state plasma sustained in helium (100 mTorr) using the centrally located coils: (*a*) the electron (top) and $He^*$ (bottom) densities, (*b*) the electric potential (top) and inductive power deposition (bottom) and (*c*) the azimuthal electric field (top) and electron source (bottom). Contour labels refer to the fraction of the maximum indicated by each value. This coil configuration produces a confined plasma. The power deposition and excited state density have their maxima near the walls due to the larger azimuthal electric field.

### 3.1. Coil placement

In this section we will discuss the spatial extent of the plasma while varying the geometry of the reactor and the configuration of the coils. Unless otherwise noted, the conditions are a power deposition of 20 W, a gas pressure of 100 mTorr and a radio frequency of 5 MHz. The three-turn coil is 6.5 cm long and has a square cross section (0.5 cm × 0.5 cm) (see figure 2). The position of the coil will be referenced by its axial midpoint ($L_c$) and its radius ($R_c$). In what will be called the standard case, the coil is centrally located ($L_c = 7.25$ cm, $R_c = 3.75$ cm).

The capacitive coupling of the plasma in a RPR reactor results from the electrostatic fields produced by the powered 'electrode' (the coil). These fields affect both the transport and the production of charged species in the reactor. The magnitude of these fields depends on the distance between the powered electrode and the earth plane and on the value of the voltage applied to the coil. The first condition is related to the geometry of the reactor and the second condition is related to the power deposition in the plasma. To isolate the effects of the inductive electric field on plasma generation and transport, we have suppressed capacitive coupling to the plasma by arbitrarily reducing the inductive voltage drop across the coil in the solution of Poisson's equation to 0.01 of its actual value. One could experimentally produce similar conditions by employing a Faraday shield around the plasma zone. We will examine the additional consequences of capacitive coupling in section 3.4.

Quasi-steady state electron (equal to the ion density) and helium metastable densities for a helium plasma using the standard conditions are shown in figure 2(*a*). The inductive power deposition and time-averaged electric potential are shown in figure 2(b), whereas the amplitude of the azimuthal electric field and ion source are shown in figure 2(c). The azimuthal electric field has its maximum at the outer radius of the discharge tube owing to the symmetry of the solenoid and to the finite skin depth of the plasma. The power deposition and ion source also have their maxima near the outer radius of the discharge tube where the azimuthal electric field is largest. The local nature of the electron source is in part a consequence of the use of the modified LFA for electron impact rate coefficients. In spite of the ion source having an off-axis maximum, the ion density has its maximum value on the axis ($2 \times 10^{10}$ cm$^{-3}$) where the plasma potential is also at its maximum (15.2 V). The metastable species density has an electron impact source having the same spatial distribution as the ions; however, its density has an off-axis maximum coincident with the source. The difference in the spatial distributions of the ions and metastable species results from a lack of volumetric sinks for the ions. Their spatial profile is therefore diffusion-dominated. In contrast, the metastable species have large volumetric sinks (electron collision quenching and collisions among metastable species) which compete with diffusion. This reactor configuration and these operating conditions produce a confined plasma.

The densities of charged particles (e, $O_2^+$ and $O^-$) and O atoms are shown in figures 3(*a*) and (b) for a plasma sustained in $O_2$ under the same conditions as for the just-discussed He plasma. The power deposition and electric potential are shown in figure 3(c). The oxygen atom densities are shown after applying both stages of accelerations which are necessary to reach their quasi-steady state densities. The maximum electron density is $1.1 \times 10^{10}$ cm$^{-3}$, whereas the positive and negative ion densities have maximum values of $1.2 \times 10^{11}$ cm$^{-3}$ and $1.1 \times 10^{11}$ cm$^{-3}$ respectively. The oxygen plasma under these conditions is electronegative, resulting in a lower plasma potential of 6 V compared to 15.2 V for the He plasma. Similarly to the helium plasma, the power deposition and electron impact source functions for ionization and excitation have their maxima near the radial wall where the azimuthal electric field has its maximum amplitude. Unlike the helium plasma, however, the plasma potential has a shallow off-axis maximum, as do the charged particle densities. These profiles result from the large volumetric sinks for ions both by ion–ion neutralization and by dissociative recombination of molecular ions. The rates of these loss processes (about $10^4$ s$^{-1}$) are commensurate to (or exceed) the loss of positive ions by diffusion. The negative ions are trapped in the plasma by the positive plasma potential and so their losses are *de facto* by volumetric processes. Also similarly

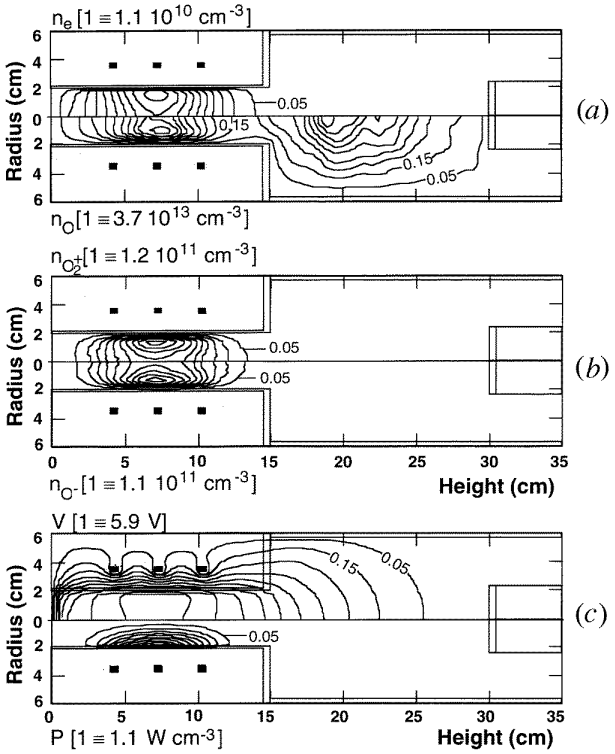


**Figure 3.** Characteristics of a quasi-steady state plasma in oxygen (100 mTorr) using the centrally located coils: (*a*) the electron (top) and O atom (bottom) densities, (*b*) the $O_2^+$ (top) and $O^-$ (bottom) densities and (*c*) the electric potential (top) and inductive power deposition. Contour labels refer to the fraction of the maximum indicated by each value. The spatial distributions of charged species more closely resemble the power deposition due to there being volumetric sinks (recombination, attachment and ion–ion neutralization). The O atoms, having low losses on surfaces, diffuse downstream, producing a remote source of radicals.

to the helium discharge, the oxygen plasma is confined. The O atoms, however, lacking significant volumetric losses in the plasma and having low losses at the walls (a reactive sticking coefficient of 0.005), diffuse downstream and fill the downstream chamber. Under these conditions, the confined plasma produces a truly 'remote' source of O atoms for the downstream chamber.

To confirm that the effects that we have just described are primarily due to inductive coupling and not to capacitive coupling leaking through our simulated Faraday shield, we reversed the polarity of the coil. Only small differences were observed in the spatial distribution of power deposition or plasma densities. We also performed calculations in which we removed the contribution of the electrostatic fields from the calculation of $E/N$ which is used to obtain rate coefficients. Again, the plasma characteristics remained nearly the same in terms of peak plasma densities and coil voltages required to sustain the plasma. The major differences were in the spatial distributions of densities in the vicinity of the substrate. In this region, the azimuthal electric field is small and, in the absence of capacitive coupling, the source of charged particles is by convection from the upstream zone. Therefore, eliminating even small ion sources by neglecting the capacitive fields in the calculation of the $E/N$ which is used to obtain rate coefficients produces a change in the downstream plasma densities. This effect, however, is minor because, under these conditions, the densities in the downstream region are several orders of magnitude lower than the peak plasma densities.

The centrally located coil for the standard case provides good confinement of the plasma in the upstream region. This confinement is, however, largely a consequence of the localized ion sources. These sources are sufficiently far from the throat of the upstream zone that charged particle losses by convection are predominantly to the walls of the narrow upstream chamber, which produces a confined plasma. The penetration of the azimuthal electric field into the downstream region is low and so the ion sources are small in that region. Since ionization rates scale exponentially with the local amplitude of the azimuthal electric field, small changes in the position of the coil can significantly alter the spatial distribution of power deposition and ion sources, and hence the confinement of the plasma.

To demonstrate this scaling, we parameterized the location of the coil over the ranges 7.25 cm $\leq L_c \leq$ 11.75 cm and 2.75 $\leq R_c \leq$ 3.75 cm. Samples of the results are shown in figure 4 in which the azimuthal electric field appears for three coil locations ranging from the standard case to a closely coupled case (the coil wrapped directly around the tube). The corresponding power deposition and electron density for a He plasma (100 mTorr, 20 W) appear in figures 5 and 6 respectively. As the coil is shifted towards the throat of the upstream plasma zone, the power deposition shifts correspondingly. The amplitude of the azimuthal electric field in the plasma decreases approximately inversely with distance from any individual coil. Therefore, as the coil approaches the discharge tube, the electric field in the plasma becomes modulated (in space) in the proximity of the coils. There is an accompanying modulation in the power deposition. The plasma density tends not to reflect the modulation in power deposition and maintains a single maximum due to the aforementioned dominance of diffusion and lack of volumetric losses.

There is a clear transition between a confined and an unconfined plasma as the coils are translated towards the throat of the plasma zone. The spatial distributions of plasma density and power deposition in figures 5(b) and 6(b) have their maximum values in the upstream plasma zone. A small shift in the location of the coil results in the location of the maximum in plasma density being shifted into the downstream chamber (figure 6(c)) while the majority of the power deposition remains in the upstream plasma zone (figure 5(c)). As the coil radius increases while keeping its axial position fixed, its proximity to the downstream chamber increases relative to the upstream chamber. The plasma then becomes unconfined. This case will be discussed in section 3.4. The transition between confined and unconfined plasmas as a function of coil position is partly explained by the relative rates of loss of ions by diffusion to the walls or out the throat of the upstream zone.

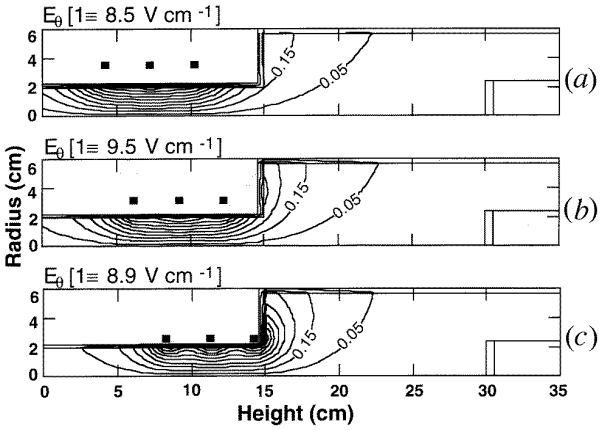


**Figure 4.** The azimuthal electric field $E_\theta$ in the quasi-steady state for plasmas sustained in He (100 mTorr, 5 MHz) using three coil configurations: (*a*) a centrally located coil ($L_c$ = 7.25 cm, $R_c$ = 3.75 cm), (*b*) an intermediate coil location ($L_c$ = 9.25 cm, $R_c$ = 3.25 cm) and (*c*) a closely coupled coil ($L_c$ = 11.25 cm, $R_c$ = 2.75 cm). Contour labels refer to the fraction of the maximum indicated by each value. Moving the coil from the central to a closely coupled location introduces large inductive fields into the downstream chamber.

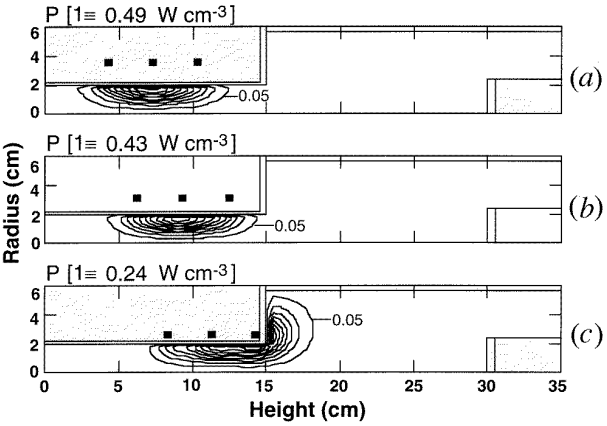


**Figure 5.** Inductive power deposition under the conditions in figure 4. Contour labels refer to the fraction of the maximum indicated by each value. Since the power deposition scales with the square of the electric field, the transition from confined to unconfined conditions resulting from fringing electric fields appears to be more abrupt.

For rare gases and for non-attaching molecular gases at low pressures, the dominant loss mechanism for ions is diffusion to the walls. The rate of diffusion scales inversely with the square of the characteristic dimension, either radially or axially. When the coil is centrally located in the upstream plasma zone, diffusion is dominated by loss to the radial walls. When the coils are moved forwards towards the throat of the upstream plasma zone, the ion source (from which ions must flow) is also moved towards the throat. As a result, the convective loss of ions from the plasma zone to the downstream chamber increases relative to diffusion losses to the radial walls. An unconfined plasma is produced when the convective loss to the downstream chamber is commensurate to or exceeds that to the radial walls of the upstream plasma zone.

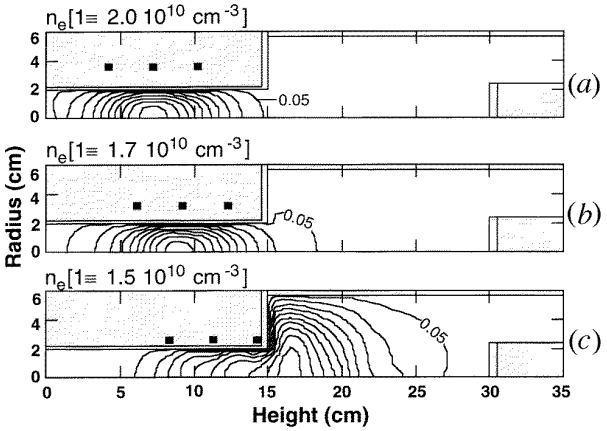


**Figure 6.** The electron density under the conditions of figure 4. Contour labels refer to the fraction of the maximum indicated by each value. The plasma rapidly undergoes transition from confined to unconfined as the azimuthal electric field penetrates into the downstream chamber.

This scaling is demonstrated in figure 7, in which we show plasma densities (He, 100 mTorr) on the axis for different values of the diameter of the upstream plasma zone ($R_P$) and downstream chamber ($R_D$) while keeping the power deposition constant. In figure 7(*a*), plasma densities are shown using the closely coupled coil located near the throat of the plasma zone as in figure 5(c). With this coil configuration, the ion source is located near the throat of the upstream plasma zone and generates ions both in the upstream and in the downstream region. As $R_P$ decreases relative to $R_D$, diffusion losses increase in the upstream plasma zone relative to those in the downstream plasma zone. The plasma density must therefore increase in the downstream zone to maintain the desired power deposition. The plasma densities as a function of $(r, z)$ position for $R_P/R_D = 0.16$ and 0.66 are shown in figure 8 for the closely coupled coils. When $R_P/R_D \leq 0.5$, the radial diffusion losses in the upstream plasma zone are sufficiently large that the plasma is nearly quenched. The diffusion losses in the downstream chamber are small by comparison, resulting in an unconfined plasma. As the diameter of the upstream plasma zone increases, the plasma is no longer quenched by diffusion losses in that region. The end result is a plasma which appears to be confined. When the coils are centrally located (as in figure 5(*a*)), the plasma remains confined over a large range of $R_P/R_D$, as shown in figure 7(b). Although the effect is not large, one sees somewhat more leakage of the plasma downstream when $R_P$ is larger relative to $R_D$ due to the larger rate of axial transport. These results are somewhat prejudiced by the fact that the total power deposition has been held constant. A confined plasma in the upstream region having a large density ($> 10^{10}$ cm$^{-3}$) may 'consume' the allocated power, leaving little to sustain the plasma downstream.

The plasma potential and ambipolar electric fields depend not only on the details of the plasma chemistry but also on the proximity of earth planes relative to the plasma. The earth planes in the model RPR are the outer wall (outside the dielectric), the substrate and, when used,

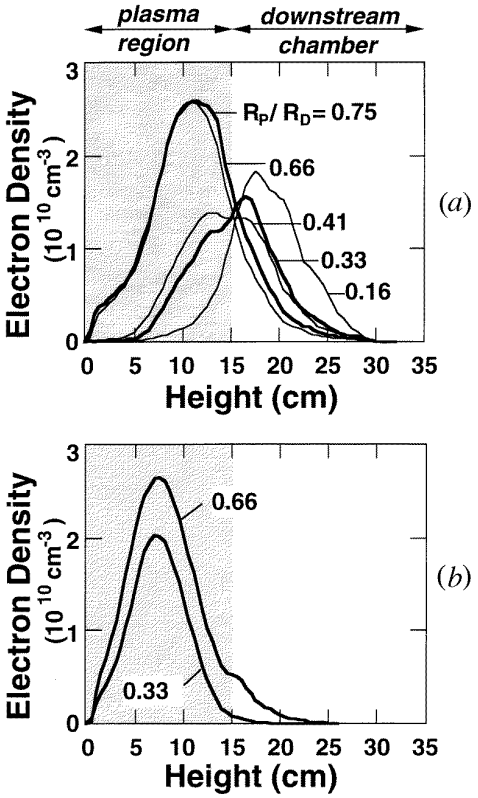


**Figure 7.** The axial electron density (He, 100 mTorr) as a function of the ratio of the radius of the plasma chamber ($R_P$) to the radius of the downstream chamber ($R_D$) for: (*a*) a closely coupled coil and (*b*) a centrally located coil. For the closely coupled coil, as $R_P$ decreases, the plasma is quenched in the upstream zone by diffusion and recombination, thereby producing what appears to be an unconfined plasma.

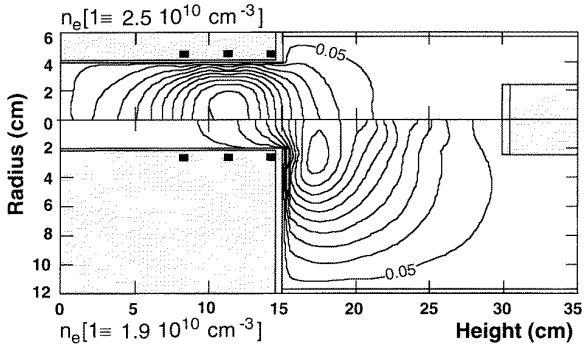


**Figure 8.** The electron density (He, 100 mTorr) for different reactor geometries using the closely coupled coils: (top) $R_P/R_D$ = 0.66 and (bottom) $R_P/R_D$ = 0.16. Contour labels refer to the fraction of the maximum indicated by each value. Under these conditions, the plasma is quenched in the upstream zone for the smaller value of $R_P/R_D$, thereby producing an unconfined plasma.

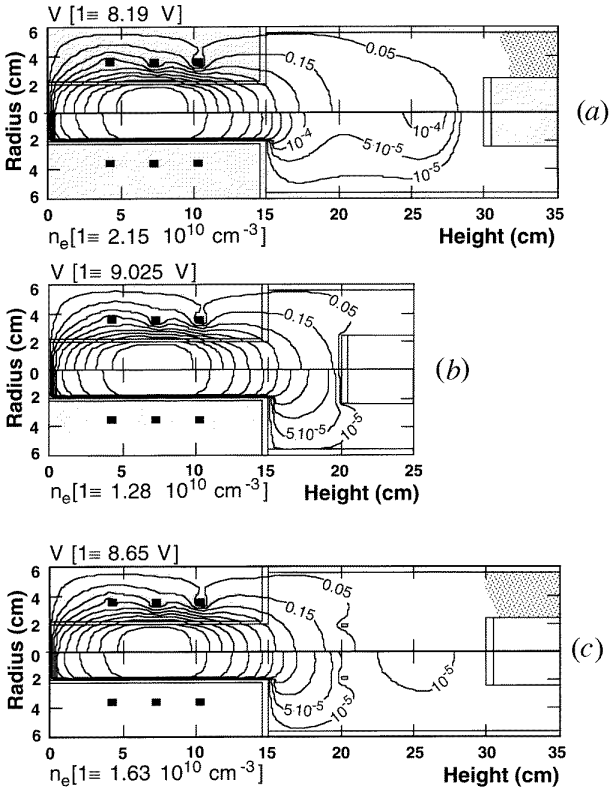


**Figure 9.** A comparison of equipotential contours and electron density for a plasma sustained in He–$SiH_4$ for different reactor geometries: (*a*) a 35 cm long reactor, (*b*) a 25 cm long reactor and (*c*) a 35 cm long reactor having an earthed injection nozzle ($z$ = 20 cm, $r$ = 2 cm). Contour labels refer to the fraction of the maximum indicated by each value. In long reactors in which the plasma decays below the ambipolar limit, regions of negative space charge are produced downstream.

the injection nozzle. The electron density and plasma potential are shown in figure 9 for discharges in a He–$SiH_4$ = 90–10 gas mixture (20 W, 10 mTorr, 13.56 MHz) in which we have changed the location of the earth plane. Plasma parameters are shown in figure 9(*a*) for the standard configuration having the earthed substrate at 30 cm, in figure 9(b) for a reactor having the earthed substrate at 20 cm and in figure 9(c) for the standard configuration having earthed nozzles (4 cm diameter) at 20 cm.

The positive plasma potential in the standard case extends to the substrate. The plasma potential, however, decays by diffusion and recombination to values below that required to sustain an ambipolar electric field before reaching the substrate. This allows the electron flux to exceed the positive ion flux at the leading end of the plasma 'plume'. The excess negative flux produces a negative plasma potential near the end of the chamber. When the earth plane is at 20 cm, the more rapid diffusion losses to the nearby substrate lower the electron density in the plasma zone relative to the standard case. The larger gradient in plasma density produces a larger ambipolar electric field and ultimately a somewhat larger plasma potential. In this case, the plasma density is sufficiently high in the vicinity of the substrate that the diffusion flux is ambipolar-limited. The plasma potential therefore remains positive everywhere.

The reactor with a remote substrate and earthed nozzles adjacent to the throat of the upstream plasma zone behaves similarly to the case with the adjacent substrate. The earth

plane wrought by the nozzles tends to help confine the plasma by confining the positive plasma potential. There is, however, 'leakage' of the plasma beyond the axial location of the nozzles. This leakage current occurs at a low plasma density which is below the ambipolar limit, thereby allowing a net negative charge to accumulate downstream which produces a small negative plasma potential.

### 3.2. Power deposition

In matters of power deposition, inductively coupled plasmas (ICPs) resemble positive column discharges. For a given $pd$ (pressure times tube diameter) product, the bulk electric field (or $E/N$) in a positive column discharge 'seeks' a value for which the electron sources are balanced by losses. For discharges in which electron loss is dominated by wall recombination and electron production is dominated by single-step processes, the axial electric field is independent of current density and therefore independent of power deposition. The axial electric field only changes during transients when the electron (or current) density moves between steady state values. A similar condition occurs in ICPs. If electron loss is dominated by wall losses, then, for a given $pd$, the azimuthal electric field in an ICP must generate a balancing electron source, which is provided by a given $E/N$. Just as in the positive column, this electric field should be independent of the circulating current and hence independent of the power deposition.

The actual situation is somewhat more complicated in ICPs since the spatial distribution of the electric field is a function of conductivity which is in turn a function of power deposition, whereas in the positive column discharge the axial electric field is uniform. For example, with higher power deposition and high conductivity, the electron source is closer to the walls, thereby producing a smaller diffusion length. Since the losses are larger, the electric field must be larger in order to compensate. A second complicating factor results from the AC nature of the excitation. The phase factor between voltage and current may be, and in most cases is, a function of power deposition. Therefore the effective $E/N$ of the plasma required for quasi-steady state operation may depend on power deposition because the phase factor changes. With AC excitation, there may also be additional power deposition from capacitive coupling which contributes to the total ionization and therefore alters the $E/N$ required for quasi-steady state operation.

Calculations were performed for power depositions of 10–100 W in an $O_2$ plasma. The maximum electron and positive ion densities as a function of power deposition are shown in figure 10. These densities are shown as a function of position for power depositions of 10 and 100 W in figure 11. With low power depositions, the plasma is more electronegative (that is, has a larger fraction of negative ions) than with high power deposition, as indicated by the large $[O_2^+]/[e]$ ratio. This is caused by the higher rate of associative detachment,

$$O^- + O \rightarrow O_2 + e \qquad (14)$$

which occurs with the higher power deposition resulting from the larger density of O atoms produced by electron impact dissociation. The end result is that the electron density increases more rapidly with power deposition than does the positive ion density.

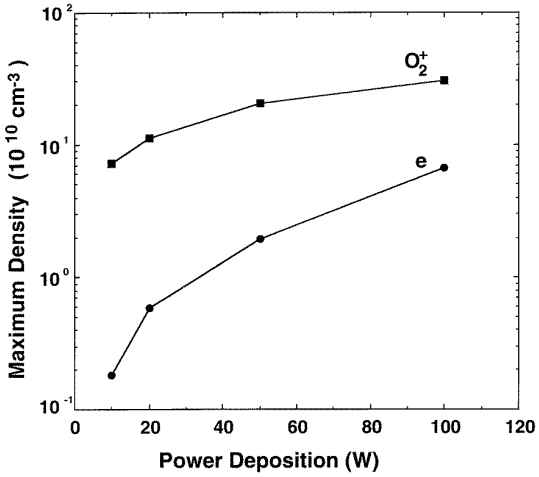


**Figure 10.** Maximum electron and $O_2^+$ densities in $O_2$ plasmas (100 mTorr, 13.56 MHz) as a function of power deposition.

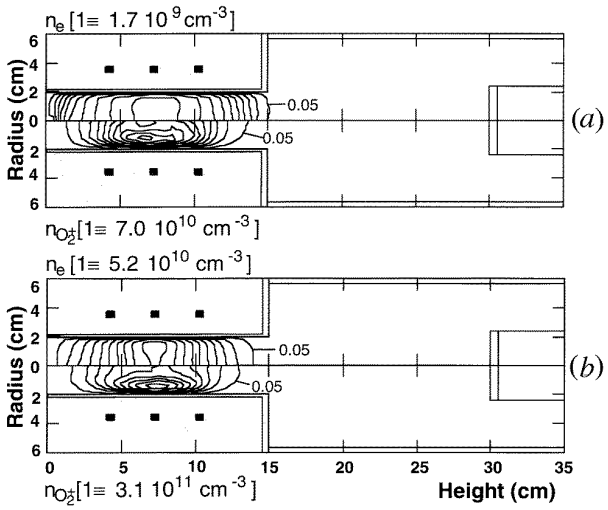


**Figure 11.** Electron and $O_2^+$ densities in $O_2$ plasmas (100 mTorr, 13.56 MHz) for different total power depositions: (*a*) 10 W and (b) 100 W. Contour labels refer to the fraction of the maximum indicated by each value. The spatial distribution of the plasma density is a weak function of the power deposition.

In both the low- and the high-power cases, the plasma remains confined to the upstream zone. The electron and ion densities are more closely correlated to the spatial distribution of the power deposition, as well as having a higher density, with the high power deposition. This scaling results from the fact that volumetric losses (electron–ion recombination and ion–ion recombination) scale as the square of the plasma density which is proportional to power deposition in recombination-dominated plasmas. Ion losses with the higher power deposition therefore occur close to the source. We also found that the phase factor between voltage and current increased with increasing power deposition.

### 3.3. The radio frequency

In RF-driven systems, the plasma conductivity is a function of excitation frequency due to the inertial motion of the electrons (equation (5)). Under the conditions of interest (gas pressure of 100 mTorr) the electron collision frequency is about $2 \times 10^8$ s$^{-1}$. Therefore, one should expect that the plasma properties will be a function of excitation frequency from a few megahertz to many hundreds of megahertz. In general, the coupling efficiency of the inductive field to the plasma should decrease over this range as the ratio of $\omega_{rf}/\nu_c$ increases. To show the expected scaling of plasma density with frequency, we made the approximation that the electron density is constant within a slab geometry of halfwidth $R$. The power deposition per unit area is then

$$P = \int_0^R \frac{\frac{1}{2}\left[E_0 \exp\left(\frac{-r}{\delta}\right)\right]^2 q^2 n_e \, \mathrm{d}x}{m_e \nu_m \left[1 + \left(\frac{\omega}{\nu_m}\right)^2\right]}$$

$$= \frac{\delta}{4} E_0^2 \frac{\left[1 - \exp\left(\frac{-2R}{\delta}\right)\right]^2 q^2 n_e}{m_e \nu_m \left[1 + \left(\frac{\omega}{\nu_m}\right)^2\right]} \qquad (15)$$

where

$$\delta = \left(\frac{2}{\omega \mu_0 \sigma}\right)^{1/2} \sim \left(\frac{1}{\omega n_e}\right)^{1/2}$$

is the collisional skin depth and $E_0$ is the electric field at the surface of the tube. In order to maintain a steady state electron density at a constant pressure the electron temperature must remain nearly constant. This implies that

$$\frac{E_0^2}{2}\left[1 + \left(\frac{\omega}{\nu_m}\right)^2\right]^{-1}$$

remain constant. With this scaling, to maintain the total power constant, in the limit of short skin depths, we expect that $n_e \simeq \omega$.

We performed a series of calculations using the closely coupled coil configuration in helium at 100 mTorr for RF frequencies in the range 5–100 MHz while keeping the power deposition constant. The peak electron density as a function of frequency is shown in figure 12. The electron density and conductivity as a function of position for frequencies 5 and 100 MHz are shown in figure 13. The mobility monotonically decreased from 5 to 100 MHz due to the increase in $\omega_{rf}/\nu_m$, as did the skin depth. The plasma density therefore increased from low frequency (5 MHz, $1.2 \times 10^{10}$ cm$^{-3}$) to high frequency (100 MHz, $1.6 \times 10^{11}$ cm$^{-3}$) in order that the total power deposition remains a constant, consistent with the previously discussed scaling. We also observed a monotonic increase in plasma potential. The spatial distribution of the plasma density was but little affected by the frequency, with the higher frequency producing somewhat better confinement. Consequently, better coupling occurs between the inductive field and the plasma in the region where the azimuthal field is high.

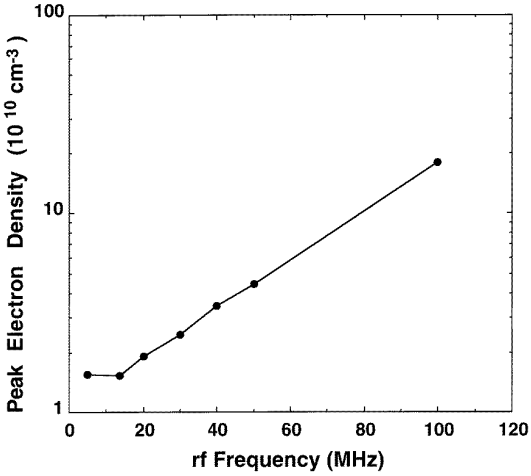


**Figure 12.** The maximum electron density as a function of the RF frequency for He plasmas (100 mTorr).

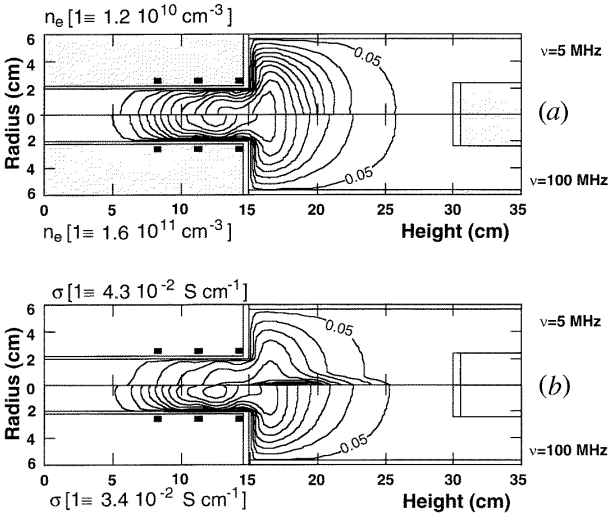


**Figure 13.** Properties of He plasmas (100 mTorr) sustained at $\nu$ = 5 MHz (top) and $\nu$ = 100 MHz (bottom) under constant power deposition: (*a*) electron density and (*b*) conductivity. Contour labels refer to the fraction of the maximum indicated by each value. The electron mobility decreases with increasing frequency due to electron inertial effects. To maintain a constant power deposition, the plasma density must increase.

### 3.4. Capacitive coupling

The results discussed in the previous sections were obtained without significant power deposition resulting from capacitive coupling. Capacitive coupling from the coils is modelled by specifying the voltage on each turn of the coil and including these values as boundary conditions in solving Poisson's equation for the electric potential. To obtain these values, an equivalent electrical circuit model was used. The coil, dielectrics and plasma were represented by an $RLC$ circuit as shown in figure 14. The $N$-turn coil is represented by $2N$ inductances $L_n$ and resistances $R_n$. The capacitance due to the dielectric wall and the air space between the coil and the dielectric wall is represented by $N$ capacitances $C_n$. The plasma resistance is $R_p$. One end

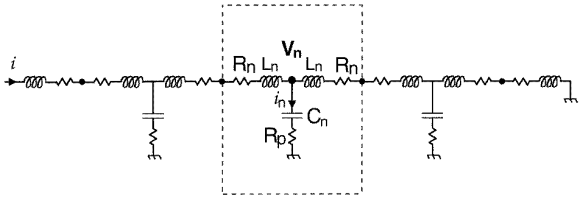


**Figure 14.** A schematic diagram of the equivalent circuit used in analysis of capacitive coupling. $V_n$ is the coil voltage, $2L_n$ is the single-turn inductance, $C_n$ is the stray capacitance to the plasma, and $R_p$ is the plasma resistance.

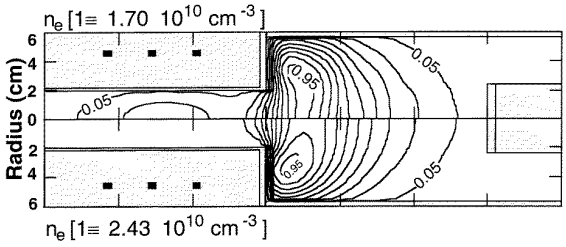


**Figure 15.** Electron densities for a He plasma at 100 mTorr without (top) and with (bottom) capacitive coupling. The coil configuration in the absence of capacitive coupling produces plasma both in the upstream and in the downstream chambers. With capacitive coupling, the plasma is quenched in the upstream zone.

of the coil is powered while the opposite end is earthed. With this circuit representation, the voltage of the last turn of the coil on the earthed end of the coil is non-zero since it is separated from earth by $L_n$. The applied voltage is normalized so that the power deposited in the plasma is a specified value, 20 W in the following cases.

A comparison of the plasma density in He (100 mTorr, 5 MHz) with and without capacitive coupling is shown in figure 15 for a centrally located coil having large radius ($L_c = 7$ cm, $R_c = 4.75$ cm). As discussed in section 3.1, the confinement of the plasma with inductive coupling depends on the location of the coil relative to the upstream and downstream chambers and the relative diameters of the chambers which determine the rates of loss by diffusion. For this choice of coil location, inductive coupling produces at best a poorly confined plasma. The plasma is sustained in the upstream chamber, but the majority of the power deposition occurs in the downstream chamber. This condition results from the remoteness of the coil from the narrow upstream chamber combined with low diffusion losses in the downstream chamber. When including capacitive coupling, the plasma is sustained in the downstream chamber while it is quenched in the upstream chamber. The stray electrostatic fields in the downstream chamber, combined with the low diffusion losses there, are sufficient to sustain the plasma. Since the power is being held constant, insufficient power remains to sustain the plasma in the upstream chamber.

## 4. Concluding remarks

A model for remote plasma reactors has been presented and the consequences of various coil configurations on confinement of the plasma have been investigated. The test reactor is a two-zone (narrow upstream, wide downstream) chamber. When operating under conditions for which capacitive coupling can be ignored (for example, using a Faraday shield) the confinement of the plasma is a sensitive function of the coil configuration and the relative radii of the upstream plasma ($R_P$) and downstream deposition ($R_D$) chambers. Typically, centrally located coils with moderate values of $R_P/R_D$ produce confined plasmas. Small values of $R_P/R_D$ may result in quenching of the upstream plasma and produce an unconfined plasma. Closely coupled coils or coils which have large radii compared to the upstream zone produce unconfined plasmas. Over the ranges investigated, power deposition, RF frequency and wall charging are not major factors in determining the confinement of the bulk plasma. These parameters may, however, affect the space charge downstream which could be of concern with respect to charging and damage of the substrate. Typically, capacitive coupling produces less confined plasmas and may lead to expulsion of the plasma from the narrow upstream zone. To ensure confinement when capacitive coupling is unavoidable, the upstream zone must be lengthened and coils recessed to reduce the magnitude of the stray electric fields to earth planes in the downstream chamber.

## Acknowledgments

This work was supported by the Semiconductor Research Corporation (Contract MJ-512), the National Science Foundation (ECS-9109326, DMR-92-01698) and Sandia National Laboratory.

## References

[1] Manos D M and Flamm D L 1989 *Plasma Etching: An Introduction* (New York: Academic)
[2] Lucovsky G, Tsu D, Rudder R and Markunas R 1991 *Thin Film Processes II* ed J L Vossen and W Kern (Boston: Academic) pp 565–619
[3] Tsu D, Parsons G N, Lucovsky G and Watkins M W 1989 *J. Vac. Sci. Technol.* A **6** 1115
[4] Qian R, Anthony B, Hsu T, Irb J, Kinosky D, Banerjee S, Tasch A and Rabenberg L 1991 *J. Appl. Phys.* **70** 3324
[5] Ventzek P L G, Hoekstra R J and Kushner M J 1994 *J. Vac. Sci. Technol.* B **12** 461
[6] Yu B W and Girshik S L 1991 *J. Appl. Phys.* **69** 656
[7] Capitelli M, Gorse C, Winkler R and Wilhem J 1988 *Plasma Chem. Plasma Proc.* **8** 399
[8] Grover F W 1946 *Inductance Calculations* (New York: Van Nostrand)
[9] Sommerer T J and Kushner M J 1992 *J. Appl. Phys.* **71** 1654
[10] Kushner M J 1992 *J. Appl. Phys.* **71** 4173